

Virus-Sized Gold Nanorods: Plasmonic Particles for Biology

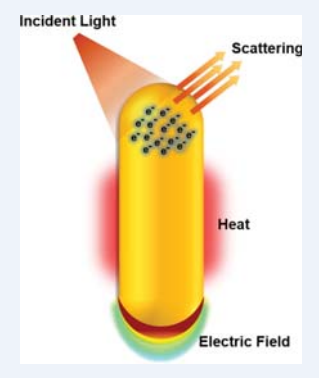
Published as part of the Accounts of Chemical Research special issue "Nanochemistry for Plasmonics and Plasmonics for Nanochemistry".

Catherine J. Murphy,*® Huei-Huei Chang, Priscila Falagan-Lotsch,® Matthew T. Gole, Daniel M. Hofmann, Khoi Nguyen L. Hoang, Sophia M. McClain, Sean M. Meyer, Jacob G. Turner, Mahima Unnikrishnan, Meng Wu, Xi Zhang, and Yishu Zhang

Department of Chemistry, University of Illinois at Urbana-Champaign, 600 South Mathews Avenue, Urbana, Illinois 61801, United States

CONSPECTUS: Plasmons, collective oscillations of conduction-band electrons in nanoscale metals, are well-known phenomena in colloidal gold and silver nanocrystals that produce brilliant visible colors in these materials that depend on the nanocrystal size and shape. Under illumination at or near the plasmon bands, gold and silver nanocrystals exhibit properties that enable fascinating biological applications: (i) the nanocrystals elastically scatter light, providing a straightforward way to image them in complex aqueous environments; (ii) the nanocrystals produce local electric fields that enable various surface-enhanced spectroscopies for sensing, molecular diagnostics, and boosting of bound fluorophore performance; (iii) the nanocrystals produce heat, which can lead to chemical transformations at or near the nanocrystal surface and can photothermally destroy nearby cells.

While all the above-mentioned applications have already been well-demonstrated in the literature, this Account focuses on several other aspects of these nanomaterials, in particular gold nanorods that are approximately the size of viruses (diameters of ~10 nm, lengths up to 100 nm). Absolute extinction, scattering, and absorption properties are compared for gold nanorods



of various absolute dimensions, and references for how to synthesize gold nanorods with four different absolute dimensions are provided. Surface chemistry strategies for coating nanocrystals with smooth or rough shells are detailed; specific examples include mesoporous silica and metal-organic framework shells for porous (rough) coatings and polyelectrolyte layer-by-layer wrapping for "smooth" shells. For self-assembled-monolayer molecular coating ligands, the smoothest shells of all, a wide range of ligand densities have been reported from many experiments, yielding values from less than 1 to nearly 10 molecules/nm² depending on the nanocrystal size and the nature of the ligand. Systematic studies of ligand density for one particular ligand with a bulky headgroup are highlighted, showing that the highest ligand density occurs for the smallest nanocrystals, even though these ligand headgroups are the most mobile as judged by NMR relaxation studies. Biomolecular coronas form around spherical and rod-shaped nanocrystals upon immersion into biological fluids; these proteins and lipids can be quantified, and their degree of adsorption depends on the nanocrystal surface chemistry as well as the biophysical characteristics of the adsorbing biomolecule. Photothermal adsorption and desorption of proteins on nanocrystals depend on the enthalpy of protein—nanocrystal surface interactions, leading to light-triggered alteration in protein concentrations near the nanocrystals. At the cellular scale, gold nanocrystals exert genetic changes at the mRNA level, with a variety of likely mechanisms that include alteration of local biomolecular concentration gradients, changes in mechanical properties of the extracellular matrix, and physical interruption of key cellular processes—even without plasmonic effects. Microbiomes, both organismal and environmental, are the likely first point of contact of nanomaterials with natural living systems; we see a major scientific frontier in understanding, predicting, and controlling microbe-nanocrystal interactions, which may be augmented by plasmonic effects.

1. INTRODUCTION

Nanoscale size and shape matter in biology: cells engulf 10-1000 nm objects by different mechanisms that depend on the object size. 1,2 Smaller colloidal nanoparticles are cleared from organisms faster than larger ones.^{3–5} Disc- or rod-shaped colloidal particles appear to evade the immune system better than spherical ones. 6,7 Viruses are nanoscale objects: 18 nm × 300 nm are the dimensions of the common tobacco mosaic

Inorganic solids on the nanoscale show size- and shapedependent properties. The mean free path of electrons in a metal at room temperature is ~10-100 nm depending on the metal, while the excitonic Bohr radius in semiconductors is $\sim 1-10$ nm. ^{9,10} Therefore, virus-sized metal nanocrystals and protein-sized semiconductor nanocrystals are expected and have been found to have fascinating size- and shape-dependent optical properties. Gold and silver nanocrystals with sizes of of roughly 5-300 nm support localized surface plasmon resonance (LSPR), which is the coherent oscillation of

Received: May 31, 2019 Published: August 2, 2019



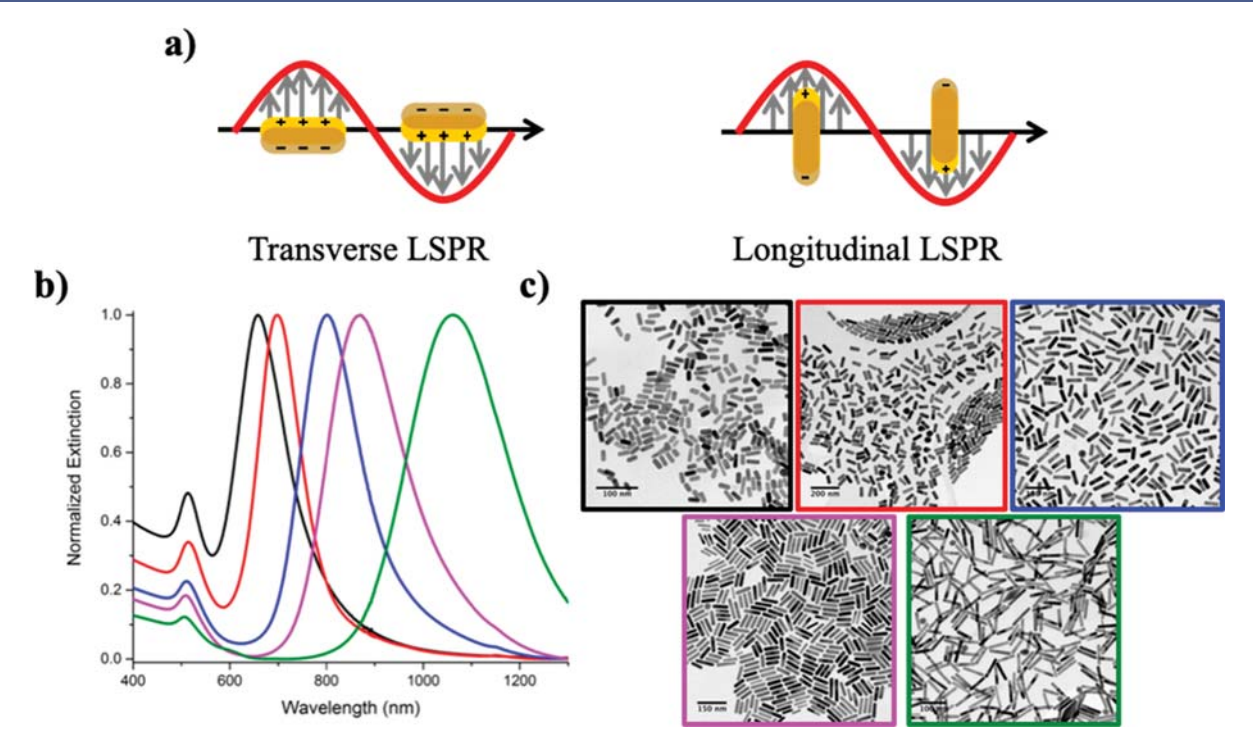


Figure 1. (a) Schematic of the localized surface plasmon resonances of gold nanorods. Reproduced from ref 14. Copyright 2016 American Chemical Society. (b) Normalized visible—NIR extinction spectra and (c) TEM images (scale bars on images) of gold nanorods with varying aspect ratios (black, AR = 2.4; red, AR = 2.7; blue, AR = 3.6; pink, AR = 4.4; green, AR = 6.1). Reproduced with permission from ref 15. Copyright 2016 Royal Society of Chemistry.¹⁵

conduction-band electrons at the metal surface upon illumination. ^{11–13} While nanospheres produce a single LSPR, it is well-known that nanorods exhibit two LSPRs: one corresponding to the transverse axis (transverse plasmon) and the other corresponding to the longitudinal axis (longitudinal plasmon). The longitudinal surface plasmon resonance can be tuned by varying either the length to width ratio (aspect ratio, AR) or the effective volume of the nanorods. For gold and silver, these LSPRs are in the visible and near-infrared (NIR) portions of the electromagnetic spectrum because of the dielectric constants of these metals (Figure 1).

Extinction in these colloidal metal nanocrystals is the sum of absorption plus elastic light scattering, and larger nanocrystals scatter more. Thus, larger colloidal metal nanocrystals can serve as effective imaging agents based solely on their elastic-light-scattering properties with no bleaching and no blinking (Figure 2).

The plasmons provide far more capabilities than elastic light scattering. Upon illumination, local electric fields are generated that allow for surface-enhanced molecular spectroscopies for local diagnostics, of which surface-enhanced Raman scattering (SERS) is the most famous, ¹⁸ and upon sufficient illumination, the large absorption cross sections of metallic nanocrystals lead to heating. ^{13,19} This plasmonic heating, described in more detail below, is sufficient to kill living cells, and there is great excitement in the field about photothermal cancer therapy that relies on this light-to-heat conversion. ²⁰

2. CONTROLLING THE ABSOLUTE DIMENSIONS OF GOLD NANORODS

The interplay of scattering and absorption by nanoscale metal particles as a function of absolute size means that the relative



Figure 2. Darkfield optical micrograph of human dermal fibroblast cells incubated with poly(allylamine)-coated gold nanospheres that are 90 nm in diameter. All of the bright spots are due to scattered light from the gold nanospheres, which were ingested by the unstained cells. Scale bar = $20~\mu m$. Reproduced from ref 17. Copyright 2013 American Chemical Society.

abilities of imaging (via scattering) and photothermal heating (via absorption) depend on the absolute particle size. Early calculations of extinction, scattering, and absorption cross sections for gold nanorods (AuNRs) and gold nanospheres (AuNSs) showed, for example, that 40 nm AuNSs scatter 6% of the light compared with that absorbed, while 80 nm spheres correspondingly scatter 68%. ¹³

The most common way to make AuNRs is via seedmediated growth methods in aqueous solution at room temperature, wherein nucleation and growth of the particle

are separated.²¹ Typically, a concentrated solution of surfactant (cetyltrimethylammonium bromide, CTAB)-stabilized gold seeds is made via the reduction of auric ions with a strong reducing agent. The seeds are then placed into a growth solution containing more surfactant, auric ions, silver ions, and a weak reducing agent to directly reduce gold ions onto the surface of the seed particles.²² The aspect ratio of the AuNRs is tunable depending on the reagent concentration. The presence of more seeds means that less gold will be available per seed, so a smaller product size dominates, and vice versa for a lower seed concentration. Overall, four different absolute size regimes of AuNRs have been reported in the literature for seemingly minor changes in synthetic protocol.^{21–25} Figure 3 represents and Table 1 summarizes these four synthetic methods used to create AuNRs of controllable aspect ratio and controlled absolute size.^{21,23–25}

3. MAKING GOLD NANORODS LOOK LIKE VIRUSES: POROUS COATINGS

The as-made AuNRs, no matter which of the four synthetic methods is used, bear a bilayer coating of the cationic CTAB surfactant on the surface. As CTAB alone is cytotoxic to at least some cell lines at micromolar concentrations, chemical strategies to remove it, cover it up, or replace it have been employed, as detailed below.

The surface coats of viruses can be considered as patterned, not homogeneous. We have been able to create AuNRs that have regularly varying "rough" surfaces by using nanoporous coatings made of inorganic materials. Porous shells around AuNRs include mesoporous silica. ^{32–34} Metal—organic frameworks (MOFs) are famed porous materials, although MOF shells are often not as uniform as their silica counterparts. ^{29,35,36}

Mesoporous silica's popularity stems from its chemical robustness, ease of synthesis, biocompatibility, and stability in a wide range of solvents. ¹⁴ We developed a synthesis of mesoporous silica-coated gold nanorods with a shell thickness that can be tuned by altering the growth solution CTAB concentration (Figure 4a,b). ³² We showed that controlling the shell thickness allows for optimization of plasmon-enhanced fluorescence of low-quantum-yield NIR fluorophores covalently anchored to the silica surface; a maximum 10-fold fluorescence enhancement was achieved with 17 nm shells. ³²

The mesoporous silica coatings with ~3 nm (and now larger) pores on AuNRs can be used for molecular uptake and photothermal release of payloads. Development of additional methods for expanding the pore size would widen the range of applications, including the sequestration, sensing, and delivery of larger biomolecules.

MOFs have extremely high surface areas, defined pore channels, and pore sizes most often less than 3 nm. ³⁸ AuNRs can be encapsulated with MOFs through either a one-pot

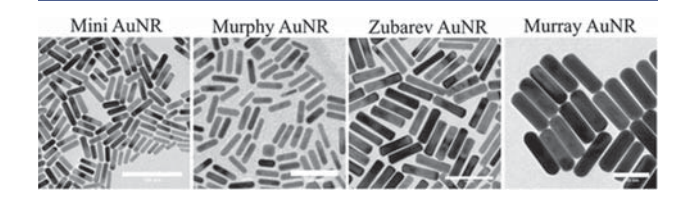


Figure 3. Representative transmission electron micrographs for the four synthesis methods mentioned in the text. Scale bars = 100 nm.

reaction of AuNRs and the MOF precursors or a layer-by-layer (LbL) process. 29,35,36

We developed an LbL process for coating AuNRs with the MOF HKUST-1 through alternating additions of copper acetate and an organic salt of the linker 1,3,5-benzenetricarboxylate. With this method, the shells are more uniform and the thickness can be precisely controlled within single nanometers (Figure 4). The HKUST-1 shell growth rate, obtained from the slope of the regression line in Figure 4d, was found to be 0.178 \pm 0.014 nm per layer. While MOFs with larger pores have been synthesized, there have not been reports of their use as shell materials around nanoparticles. In order to have larger mesopores, the MOF shell has to be postsynthetically etched, which in turn results in the loss of the desirable defined pore channels. AuNR@MOF materials have demonstrated unique capabilities as combined photothermal and chemotherapeutic agents through stimuli-responsive drug release. 35,39

4. MAKING GOLD NANORODS LOOK LIKE VIRUSES: SOFT ORGANIC COATINGS

Gold nanorod surface modification can be achieved using LbL deposition of polyelectrolytes (PEs), which increases the thickness of the surface layer and also allows the reversal of surface charge. This approach, similar to standard LbL techniques, ⁴⁰ involves alternatively adding anionic and cationic PE layers onto the oppositely charged AuNRs through electrostatic and hydrophobic interactions. For optimal PE coating, the polymers should have a chain length comparable to the dimensions of the nanoparticles, and the ionic strength should allow the polymers to be in a flexible, extended conformation. If these considerations are ignored, the nanoparticles can flocculate as a result of multimer formation due to bridging, polymer rigidity, and/or insufficient electrostatic repulsion. ⁴¹

UV—vis spectroscopy can be used to monitor the formation of PE coatings on AuNRs (Figure 5), where shifts in the plasmon peak maximum are observed in an alternating fashion after each successive coating of the anionic PE poly(acrylic acid) (PAA) and cationic PE poly(allylamine hydrochloride) (PAH). These shifts are caused by the change in refractive index of the surrounding medium. It is important to note the particle loss after each layer-by-layer coating due to the removal of excess PE by centrifugation; successful coating is limited to about 10 layers. The most effective way to characterize these successive PE depositions is by measuring the ζ potential to confirm the charge reversal after each successful coating (Figure 5c). The PE layer thickness (h) can be extracted from measurements of the hydrodynamic diameter from dynamic light scattering (DLS) (Figure 5d): 42

$$d_{\rm H} = \frac{k_{\rm B}T}{3\pi\eta D_{\rm t}} \tag{1}$$

$$D_{\rm t} = \frac{k_{\rm B}T \ln\left(\frac{L}{d_{\rm CS}}\right) + C_{\rm t}}{3\pi\eta L} \tag{2}$$

$$C_{\rm t} = 0.312 + 0.565 \left(\frac{d_{\rm CS}}{L}\right) - 0.100 \left(\frac{d_{\rm CS}}{L}\right)^2$$
 (3)

$$L = L_{\text{AuNR}} + 2h \tag{4}$$

Table 1. List of AuNR Properties for Four Different Synthetic Methods in the Literature (Which We Name Mini, Murphy, Zubarev, and Murray); ^{21,23-25} Each Synthetic Method Produces Nanorods with Tunable Aspect Ratio

	dimension r L ×			reported SPR	range (nm)		(% of total ction)	mola	extinction (M ⁻¹ cr	coefficients, ε
AuNR type ^a	L (nm)	W (nm)	aspect ratio range	longitudinal	transverse	exptl ^b	calcd ^c	AR	λ (nm)	ε
Mini	20-100	5-10	2-11+	600-1300	504-523	N/A	0.5-2.5%	2.2	607	3×10^{8}
								3.8	793	2×10^{8}
								8.2	1040	9×10^{8}
Murphy	20-100	10-20	2-5	650-950	504-523	20-30%	7-10%	2	605	2.5×10^{9}
								2.9	728	3.9×10^{9}
								3.5	785	4.6×10^{9}
								4.5	845	5.5×10^{9}
Zubarev	50-100+	10-30	2-7	770-1160	504-523	25-40%	20-40%	4	800	1.6×10^{10}
Murray	70-190	15-75	2-7	650-1150	504-540	30-50%	30-70%	2.9	787	7.91×10^{10e}
								3.6	794	4.6×10^{10e}

References listed below are in the order of Mini, Murphy, Zubarev, then Murray rods. ^aSynthesis, optical, and physical properties: 23, 21, 24, 25. ^bExperimental scattering %: n/a, 27, 27, 30. ^cTheoretical scattering %: 26, 13, 13, 30. ^dExtinction coefficients: 23, 28, 29, 31. ^cExtinction coefficients reported are for AuNRs with silica coating. ^fSPR = surface plasmon resonance.

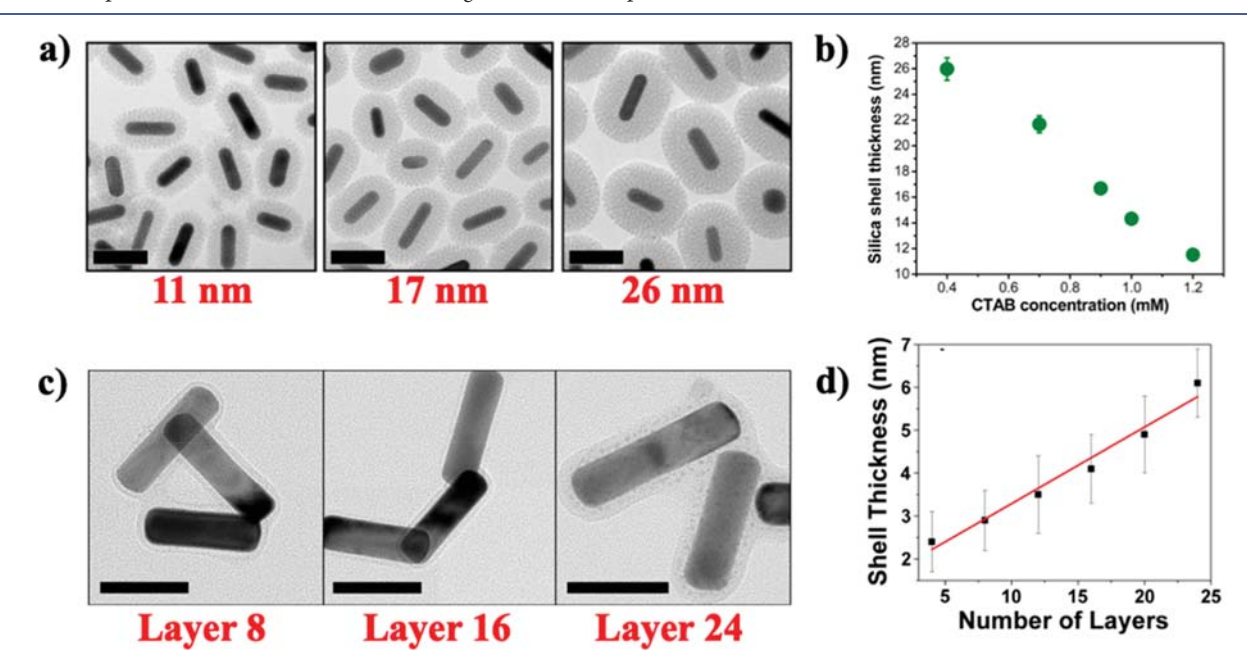


Figure 4. AuNRs with porous shells. (a) Transmission electron micrographs of silica-coated AuNRs with varying shell thicknesses. Scale bars = 50 nm. (b) Silica shell thickness vs CTAB concentration in the growth solution. (c) Transmission electron micrographs of HKUST-1-coated gold nanorods. Scale bars = 50 nm. (d) HKUST-1 shell thickness as a function of the number of layers deposited. Reproduced from (a, b) ref 32 and (c, d) ref 29. Copyright 2014 and 2018, respectively, American Chemical Society.

$$d_{\rm CS} = d_{\rm AuNR} + 2h \tag{5}$$

where $d_{\rm H}$ is the hydrodynamic diameter due to the translational diffusion of the AuNRs, $k_{\rm B}$ is the Boltzmann constant, T is absolute temperature of the sample solution, η is the viscosity of the solution, $D_{\rm t}$ is the translational diffusion constant, L is the total length of the coated AuNR, $d_{\rm CS}$ is the total diameter of the coated AuNR, and $L_{\rm AuNR}$ and $d_{\rm AuNR}$ are the average length and diameter of the bare AuNRs measured from transmission electron micrographs.

LbL PE deposition is a facile method to functionalize AuNR surfaces with controlled surface charge and coating thickness. This also allows for loading of molecules on or within the PE layers to make AuNRs more like soft, organic nanoparticles. In addition, molecular self-assembled monolayers (SAMs) can also be employed to modify the surface of AuNRs in order to

make them more "viruslike". Hydrophobic octadecanethiol-coated AuNSs functionalized with lipids, or surfactants, form a "hybrid" lipid bilayer on AuNSs.⁴⁴ The nonpolar tail of the lipid/surfactant associates with the nonpolar chain of the octadecanethiol SAM.

5. WHAT DOES THE MOLECULAR LANDSCAPE LOOK LIKE ON A GOLD NANOCRYSTAL? LIGAND DENSITY ANALYSIS

Viruses are miracles of molecular-scale ordering over tens or hundreds on nanometers. Molecular SAMs have been employed to modify the surface of nanoparticles. SAMs of thiolated molecules on gold surfaces are well-known and are usually considered to be "molecularly smooth". 45 On flat gold surfaces, small thiols have ligand densities of 2–4 molecules/

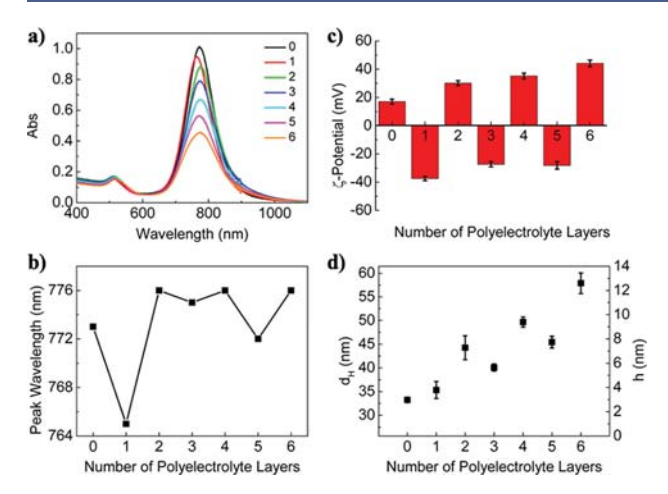


Figure 5. LbL surface coating of AuNRs with PAA and PAH. (a) Visible spectra of AuNRs as a function of the number of alternating PE coatings: curve 0 = as-prepared AuNRs; curves 1, 3, and 5 = PAA; curves 2, 4, and 6 = PAH. (b) Longitudinal plasmon peak maximum for AuNRs as a function of the number of PE layers. (c) ζ potential data for AuNRs as a function of PE coating. (d) Effective hydrodynamic diameters $(d_{\rm H})$ of AuNRs for various numbers of PE coatings as measured by DLS and equivalent thicknesses of PE layers (h) as calculated using eqs 1–5. The alterations in PE layer thickness are thought to result from different degrees of hydration within the layers. Reproduced from ref 42. Copyright 2013 American Chemical Society.

nm², while $\sim \! 1\!-\! 2$ nm gold nanocrystals have been reported to have 9 thiol molecules/nm² (Table 2). $^{46-54}$

In Table 2 we show literature ligand density values for different SAMs on gold. In our own work, 46 we have found that the ligand density of a long-chain thiol with a bulky headgroup varies as a function of the AuNS diameter, with the smallest particles having the highest ligand densities (Figure 6b), yet the headgroup mobility, as determined by NMR spectroscopy, is largest for the smallest nanoparticles (Figure 6a,c). In concert with molecular dynamics simulations, we have reconciled these seemingly contradictory results by realizing that the bulky quaternary ammonium headgroup of the ligand jams for particle core sizes larger than 10 nm, but ligand flexibility on smaller particles allows for both higher packing densities and more headgroup mobility (Figure 6d).

6. BIOMOLECULAR CORONAS AND THEIR RESPONSE TO PLASMONIC HEATING

The surfaces of nanoparticles can be altered by their introduction into biological or natural environments, where-upon they acquire coatings of biomolecules, called coronas. The formation and composition of these coronas are dependent upon both the physical and chemical properties of the nanoparticles, such as size, shape, and surface chemistry.

The denaturation behavior of a protein might be a useful predictor of its adsorption behavior toward AuNSs. ⁵⁶ We studied protein adsorption to anionic citrate-capped AuNSs and to cationic PAH-wrapped AuNSs for three proteins: α -amylase (A-Amy), β -lactoglobulin (BLG), and bovine serum albumin (BSA). ⁵⁶ Langmuir adsorption isotherm results showed that the affinities for citrate-capped AuNSs were ordered as BSA > BLG \gg A-Amy, while PAH-coated AuNSs displayed little affinity for these proteins, in accord with electrostatics. ⁵⁶ Changes in the secondary structure of proteins

on AuNSs did follow the trends predicted by acid denaturation characteristics for both citrate- and PAH-AuNSs. Mile protein coronas have drawn much attention, other biomolecular coronas such as lipid coronas are equally important. We recently developed an LC/MS/MS method to assess the degree of lipid corona formation on 14 nm AuNSs upon incubation with lipid vesicles. We compared cationic MTAB- and PAH-AuNPs, where MTAB displays a quaternary ammonium group to the solvent while PAH displays primary amines. Cationic MTAB-AuNPs and PAH-AuNPs extracted 60–95% of the lipids available (Figure 7), while anionic citrate-AuNPs extracted almost none. The primary amine polymer surfaces extracted more lipids than the quaternary ammonium surfaces.

The property of heat generation upon light excitation makes plasmonic nanoparticles extremely interesting for nanomedicine applications, such as controlled photothermal release of molecules, and for photothermal therapy. This heat generation phenomenon is explained by the strong absorption of incident light from an external source (e.g., NIR laser) by the plasmonic particles, leading to the excitation of free electrons. Via electron—electron collisions, hot electrons are created. Then the fast transfer of energy from the hot electrons to phonons via electron—phonon coupling generates heat with electron temperatures rising in the vicinity of plasmonic nanoparticles by a few tens to thousands of degrees (on short time scales) (Figure 8).

The composition of protein coronas formed on AuNRs after incubation in fetal bovine serum (\sim 5000 different proteins at millimolar concentrations) differs significantly when subjected to plasmonic heating compared with conventional thermal heating. Photoinduced heating led to an increase in several biologically relevant proteins bound to the particles, including serum albumin, α -2-HS-glycoprotein precursor, apolipoprotein A-II precursor, and apolipoprotein C-III precursor, which have the potential to affect blood circulation time and the ability of particles to cross the blood—brain barrier. Understanding how laser irradiation affects the corona composition of plasmonic nanoparticles and therefore their interactions with other biological entities is vital for successful photothermal drug delivery and cancer therapy.

The photothermal effect produced by plasmonic nanoparticles (NPs) upon irradiation has been explored for the thermally induced release of molecules (e.g., drugs, DNA, siRNA, proteins) into cells for targeted therapeutics. This strategy could significantly enhance the treatment efficacy while reducing/eliminating the undesirable side effects of drugs and prevents degradation of the therapeutic payload. However, cargo release using photothermal heating of plasmonic NPs works only if the molecule—NP interaction is exothermic in nature, following Le Chatelier's principle. By investigating the interactions between protein/PE-wrapped AuNR pairs that had either endothermic or exothermic associations, we found that the endothermic system increased protein absorption to the surface, while the opposite was observed in the exothermic one (Figure 9) according to:

endothermic:

protein + NP + heat → protein-NP complex

exothermic:

protein + NP \rightarrow protein-NP complex + heat

Table 2. Summary of Ligand Densities of Representative SAMs in the Literature

Ligand type	Gold surface	Ligand density / molecule per nm ² (method)		
CH ₃ SH	Flat Au(111) surface	4.65 (XPS)	47	
3-Mercaptopropionic acid (MPA)	AuNSs (13.2 \pm 1.4 nm to 26.2 \pm 4.4 nm)	6.3 ± 0.6 (ICP-MS)	48	
6-Mercaptohexanoic acid (6-MHA)	AuNSs (13.0 ± 1.3 nm)	4.6 ± 0.1 (XPS)	49	
8-Mercaptooctanoic acid (MOA)	AuNSs (13 ± 1 nm and 31 ± 1 nm)	4.0 ± 0.1 (qNMR after aqua regia digestion)	50	
11- Mercaptoundecanoic	AuNSs (13 ± 1 nm and 31 ± 1 nm)	4.4 ± 0.1 (qNMR after aqua regia digestion)	50	
acid (MUA)	AuNSs $(13.2 \pm 1.4 \text{ nm})$ to $26.2 \pm 4.4 \text{ nm})$	5.7 ± 0.1 (ICP-MS)	48	
	AuNSs (12.6 ± 1.2 nm)	5.0 ± 0.1 (XPS)	49	
Dodecanethiol HS CH ₃	AuNSs (2.4 ± 0.1 nm)	9.30 (SAXS and elemental analysis)	51	
Mercaptohexadecanoic acid (16-MHA)	AuNSs (13.2 ± 1.4 nm) to 26.2 ± 4.4 nm)	5.3 ± 0.2 (ICP-MS)	48	
mercaptohexadecyl)tri methylammonium bromide (MTAB)	200 2000 - 200 - 200 - 200	3.0 ± 0.8 to 6.5 ± 1.8 (in situ qNMR) $1.8~\pm~0.4~\text{to}~4.8~\pm~1.1$ (qNMR after I_2 digestion)	46	
SH-PEG ₄ -COOH	AuNSs $(13.2 \pm 1.4 \text{ nm})$ to $26.2 \pm 4.4 \text{ nm})$	$5.0\pm0.3(\text{ICP-MS})$	48	
SH-PEG7-COOH	AuNSs $(13.2 \pm 1.4 \text{ nm})$ to $26.2 \pm 4.4 \text{ nm})$	4.3 ± 0.4 (ICP-MS)	48	

Ligand type	Gold surface	Ligand density / molecule per nm ² (method)	Re
mPEG-SH (average Mw=1000 Da)	AuNSs (13 \pm 1 nm and 31 \pm 1 nm)	2.2 ± 0.1 (qNMR after aqua regia digestion)	50
H ₂ N-PEG-SH (average Mw=5000 Da)	PVP-AuNCs (30 nm in edge length)	0.61 (Fluorescamine-based assay, total PEGs) 0.19 (FITC-labeling assay, active PEGs)	52
	PVP-AuNCs (50 nm in edge length)	0.85 (Fluorescamine-based assay, total PEGs)	52
	PVP-AuNCs (60 nm in edge length)	1.36 (Fluorescamine-based assay, total PEGs)	52
	CTAC-AuNSs (40 nm)	0.41 (Fluorescamine-based assay, total PEGs) 0.22 (FITC-labeling assay, active PEGs)	52
	Cit-AuNSs (42 nm)	1.63 (Fluorescamine-based assay, total PEGs) 1.01 (FITC-labeling assay, active PEGs)	52
	CTAB-AuNRs (80 nm × 22 nm)	0.052 (Fluorescamine- based assay, total PEGs) 0.029 (FITC-labeling assay, active PEGs)	52
Thioctic acid	AuNSs (12.3 ± 1.2 nm)	2.2 ± 0.1 (XPS)	49
Mercaptobenzimid- azole	AuNSs (13 nm)	3.4 (Ratiometric SERS)	53
Oligonucleotides-SH	AuNSs (10 nm to 200 nm)	0.06 to 0.21 (Oligreen assay after CN ⁻ digestion)	54

Therefore, Le Chatelier's principle can be applied to the nanoscale to predict protein—NP interactions and the successful release of biomolecules from the surface of

nanoparticles upon irradiation, even when more complex biological environments are considered.

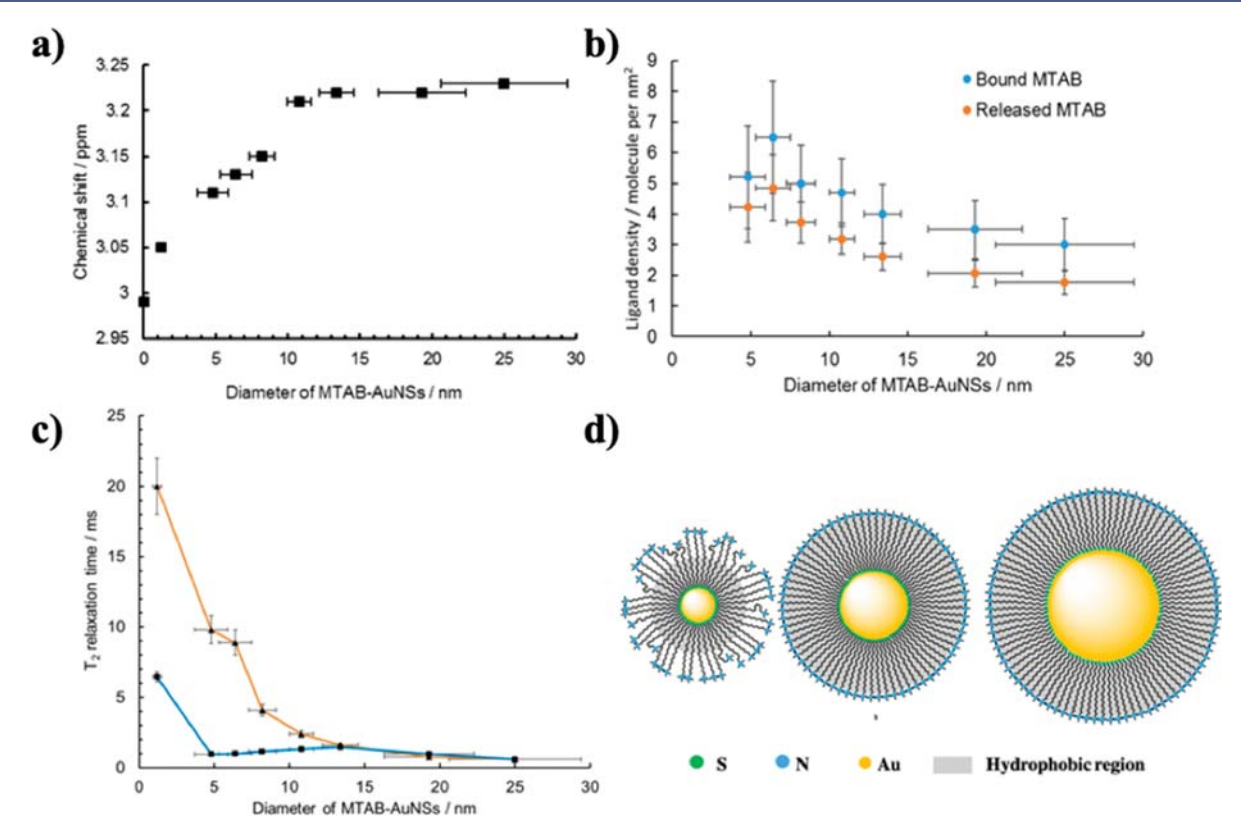


Figure 6. Graphs of (a) the chemical shift of MTAB headgroup protons, (b) the MTAB ligand density from two independent methods, (c) T_2 (orange line) and T_2^* (blue line) relaxation times, and (d) MTAB conformation and packing as functions of AuNS diameter. Reproduced from ref 46. Copyright 2019 American Chemical Society.

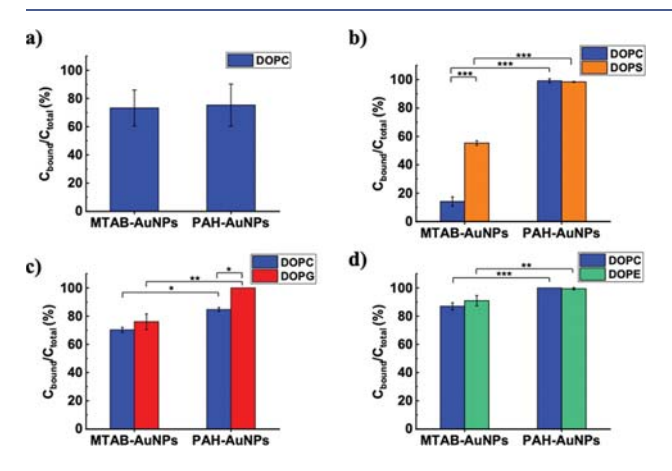


Figure 7. $C_{\rm bound}/C_{\rm total}$ percentages after pull-down separation of AuNP pellets, based on LC-MS/MS quantification. The lipids were (a) DOPC, (b) 9:1 DOPC/DOPS, (c) 9:1 DOPC/DOPG, and (d) 9:1 DOPC/DOPE. Bar heights represent mean values; error bars correspond to one standard deviation for triplicate runs from the same batches of nanoparticle and lipid vesicle solutions. Asterisks correspond to the following p values using ANOVA followed by post-hoc multiple comparisons test: *, p < 0.05; **, p < 0.01, ***, p < 0.001. Reproduced from ref 57. Copyright 2018 American Chemical Society.

7. PHOTOTHERMAL KILLING OF PATHOGENIC BACTERIA

Multidrug-resistant (MDR) bacteria present a great threat to public health. The photothermal properties of gold nanocryst-

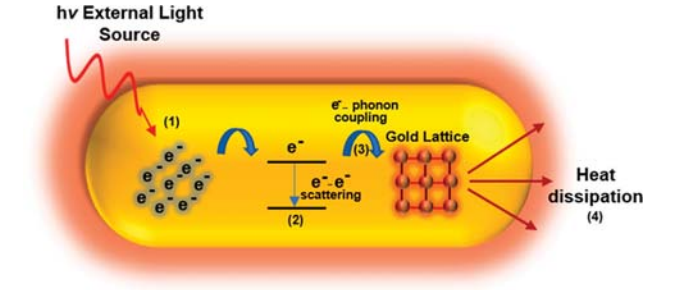


Figure 8. Schematic representation of the photothermal heating process in gold nanoparticles: (1) photoexcitation of free electrons in the plasmon band; (2) relaxation via electron–electron scattering, leading to a rapid increase in the nanoparticle surface temperature; (3) heat transfer from the electrons to the gold lattice phonons via electron–phonon coupling; (4) heat dissipation from the gold lattice to the medium surrounding the plasmonic nanostructure through phonon–phonon interactions.

als have also been exploited to kill pathogenic bacteria, including MDR ones. We applied PE-coated AuNRs conjugated with antibodies as photothermal agents to selectively kill the Gram-negative MDR bacterium *Pseudomonas aeruginosa*⁶² (Figure 10). Plasmonic excitation of AuNRs led to a significant decrease in cell viability, and the irradiated cells showed irreparable cell membrane damage. Gold nanoparticle-mediated photothermal killing is effective against other different strains of bacteria, from Gram-positive to Gramnegative, ⁶³ and is a promising strategy to destroy bacterial biofilms. ⁶⁴

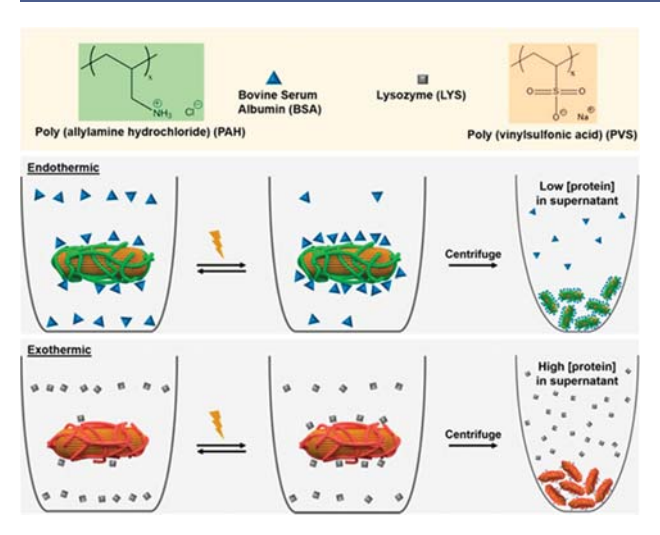


Figure 9. Cartoon showing the behavior of proteins on nanoparticle surfaces given the thermodynamics of each system. The behavior is tested by measuring the protein concentration in the supernatant following NIR laser irradiation. Endothermic reactions favor the complex upon addition of heat, producing less protein in the supernatant, while exothermic reactions favor free reactants, leading to higher protein concentration in the supernatant. Reproduced from ref 61. Copyright 2017 American Chemical Society.

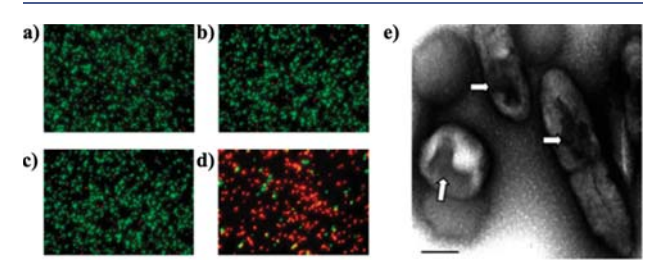


Figure 10. Selective photothermal killing of pathogenic bacteria using AuNRs. The left panel shows the viability of *Pseudomonas aeruginosa* cells with attached AuNRs following exposure to NIR light: (a) control cells without nanorods or NIR exposure; (b) cells without nanorods exposed to NIR light; (c) cells with nanorods and no NIR exposure; (d) cells with nanorods and exposed to NIR light for 10 min. Green-fluorescent cells are alive, while red-fluorescent cells are dead or compromised. (e) TEM image (30000×) of *P. aeruginosa* cells with attached antibody-conjugated nanorods following 10 min exposure to NIR light. The arrows indicate irreparable damage in the bacterial cell surface. Scale bar is 500 nm. Adapted from ref 62. Copyright 2008 American Chemical Society.

8. VIRUS-SIZED GOLD PARTICLES AND INTERACTIONS WITH BIOLOGICAL SYSTEMS

Understanding of the interactions of nanoparticles with biological systems is essential for safe human exposure to nanoscale materials. By investigating the interactions of gold nanocrystals with the extracellular matrix and monitoring cell behavior, we noticed changes in the mechanical properties of the extracellular matrix when these nanoparticles were added to the system, promoting the migration of cancer cells, which is a concern.⁶⁵

Surface chemistry is one of the major intrinsic parameters governing nanocrystal toxicity, playing a key role in nano—bio interactions. Transcriptomic analyses performed by us on two cell types exposed to four differently coated AuNSs showed significant changes in the expression of genes involved in

pathways such as cell proliferation, inflammation, and cell death according to their surface chemistry. Surprisingly, the biomimetic lipid-coated AuNPs affected the highest number of genes, highlighting the complexity of nano-bio interactions.⁶⁶

Currently, very little is known about the long-term effects of nanocrystal exposure on living systems. To shed light on this issue, we assessed the effects of a low dose of AuNSs and AuNRs with different surface chemistries to human cells under chronic and acute exposures after 20 weeks.⁶⁷ Although no significant impact on cell viability was observed, analysis at the molecular level revealed that the nanocrystals induced long-term changes in the expression levels of cell stress response genes. Intriguingly, acute exposure (24 h) led to a sustained cell stress response that was detectable even 20 weeks after the stimulus, indicating that the cells did not recover properly over time.⁶⁷ However, upon chronic exposure the cells adopted an altered state in response to the continual stress (nanoparticles).⁶⁷ Therefore, cells adapt to nanocrystal stresses over time.

In vivo data on the fate, bioaccumulation, and toxicity of gold nanoplatforms over long time periods are still lacking. The El-Sayed group investigated the long-term toxic effects of AuNRs in mice, and although no evident toxicity was found at 15 months postinjection, most of the AuNRs still remained inside the hepatocytes and spleen cells. 68

VIRUS-SIZED GOLD NANOPARTICLES IN THE ENVIRONMENT: FROM SOIL TO BACTERIA

Nanoenabled consumer products began to appear in the marketplace in 1999. These nanomaterials can be released into ecosystems through air, soil, sludge, wastewater, seawater, and freshwater from the beginning of manufacturing to the disposal of nanomaterial-enabled products. To understand how these engineered nanomaterials interact with ecosystems, we have investigated gold nanoparticle (AuNP) distributions and effects on soil, ⁶⁹ groundwater, ⁶⁹ and microbiomes. ^{70,71}

Prior to studying NP influences on microbiomes, we examined how changes in the physicochemical properties of AuNPs affect their soil retention and colloidal stability in groundwater. AuNPs with different shapes, surface chemistries, and charges were passed through soil columns. Upon elution with simulated groundwater, 4-fold more spherical AuNPs were retained in the soil column compared with rodshaped counterparts for various surface chemistries. However, we found that regardless of charge, spherical AuNPs aggregated within several hours when incubated with simulated groundwater. We also observed that compared with PEwrapped AuNPs, AuNPs wrapped with relatively labile capping agents were more susceptible to irreversible aggregation in simulated groundwater.

We have evaluated NP toxicity and the interaction of NPs with diverse bacteria. In one study, we chose a panel of bacteria present in diverse habitats. To Each bacterium possesses a unique cell wall structure made up of either smooth or rough lipopolysaccharides (LPS) with different phosphate units and charges. We observed that bacteria with smooth LPS bound more AuNPs than those with rough LPS. Toxicity to bacteria was observed even though NPs did not enter the bacteria; again, compromised cell membranes appeared to be one of the root causes. In another study, we utilized metagenomics and found that AuNSs and AuNRs, at low doses for 56 days, altered the composition of microbial communities and increased levels of antibiotic resistance genes (ARGs). This

result is consistent with a study showing that 40 ARGs were significantly enriched in the presence of rare-earth oxide nanoparticles. 72

As gold is of low natural abundance in the environment and inductively coupled plasma mass spectrometry (ICP-MS) detection limits are at the parts per trillion level, we used ICP-MS to measure the distributions of both initially cationic and anionic AuNRs in model estuarine mesocosms at doses that correspond to that of a viral "infection" in an ecosystem.^{73,74} After 2 weeks of exposure, the microbial biofilms were found to be the main sink in the living food web, and the initial surface chemistry of the nanorods did dictate the ultimate environmental distributions.^{73,74} On top of these observed changes in microbial community composition as a function of AuNP exposure, recent work⁷⁵ has shown that bacterial biofilms associated with an aquatic plant can spontaneously produce sufficient cyanide to oxidize gold according to

$$4Au + 8CN^{-} + O_2 + 2H_2O \rightarrow 4[Au(CN)_2]^{-} + 4OH^{-}$$

Thus, another mode of biological damage that involves bacteria is the unexpected production of more inherently toxic gold ions, compared with elemental gold, by microbial biofilms under certain conditions.

10. CONCLUSIONS AND FUTURE DIRECTIONS

This Account has surveyed a great deal of ground: synthesis, surface chemistry, biomolecule—surface interactions, cellular interactions, and environmental fate and impacts of AuNPs. Much has been done, and much remains to do. What are the most impactful future directions?

Patchy Particles: Measurement and Impact

Just as virus particles display ordered yet varied surfaces, colloidal nanocrystals could in principle display similar functionalities as opposed to "monoculture" surfaces. The synthesis of nanocrystals bearing multiple functional groups is reasonably straightforward, but the measurement of individual particle "surface identities" is not at all straightforward. With the advent of improving single-particle, single-molecule, and cryogenic electron microscopy methods, progress is likely to be rapid in this area. In principle, one could design artificial nanocrystals that have both the symmetry and variety of natural viral particles. However, even for simple "monoculture surface" systems, the nanocrystal diameter affects the molecular display.⁴⁶

Microbiomes Plus Nanoparticles

Of all the biological systems that could interact with nanocrystals, we believe that bacteria are the most important. Microbiomes are abundant in the open environment and within organisms and might be the first point of contact between an engineered nanomaterial and anything (soil, gastrointestinal tract, etc.). We speculate that one reason for the failure of many nanoparticle-enabled drug delivery experiments in organisms is a failure to take into account the relevant microbiomes.⁷⁶ Detailed understanding and prediction of how nanocrystals are processed by microbiomes and impact their resident bacterial populations are key research areas for future study.

Plasmonic Biology

Just as optogenetics has opened new doors in understanding and controlling especially the brain, can "plasmon genetics" be a new field of scientific inquiry to understand and control cellular and organismal functions? As organisms regulate temperature far more closely than they regulate light absorption, this is a fanciful suggestion. Nevertheless, as more data accumulate about cellular responses to nanoparticle exposure that include turning on "unfolded protein response" genes, ⁶⁷ one can imagine that the fundamental disordering of protein structure due to nanocrystal binding could have cascading impacts on biological function at higher levels.

AUTHOR INFORMATION

Corresponding Author

*E-mail: murphycj@illinois.edu.

ORCID ®

Catherine J. Murphy: 0000-0001-7066-5575 Priscila Falagan-Lotsch: 0000-0002-0849-2682 Daniel M. Hofmann: 0000-0002-9761-5719 Khoi Nguyen L. Hoang: 0000-0002-3822-4216 Sophia M. McClain: 0000-0003-4407-8080 Jacob G. Turner: 0000-0001-6687-1536 Xi Zhang: 0000-0001-5777-2368

Notes

The authors declare no competing financial interest.

Biographies

Catherine J. Murphy holds the Larry R. Faulkner Endowed Chair in Chemistry at the University of Illinois at Urbana—Champaign (UIUC). She earned two B.S. degrees from UIUC in 1986, one in Chemistry and one in Biochemistry. Her Ph.D. (1990) is from the University of Wisconsin-Madison with A. B. Ellis. After postdoctoral fellowships at the California Institute of Technology with J. K. Barton (1990—1993), she joined the faculty of chemistry and biochemistry at the University of South Carolina. After rising through the faculty ranks at South Carolina (1993—2009), she was recruited back to UIUC in 2009.

Huei-Huei Chang is from Taipei, Taiwan, and received a B.A. degree in Chemistry from Iowa State University. She is currently a Ph.D. candidate in the Murphy group at UIUC. Her research interests focus on how the size and surface chemistry of gold nanoparticles affect cellular responses.

Priscila Falagan-Lotsch is a research scientist in the Murphy research group at UIUC. She received her B.S. degree in Biomedical Science from the Federal University of the State of Rio de Janeiro in Brazil and completed her M.S. (2004) and Ph.D. (2008) at the Rio de Janeiro State University in Brazil with a period at the International Agency for Research on Cancer (WHO/France). Prior to joining the Murphy group in 2015, she worked as a researcher at the Brazilian National Institute of Metrology, Quality and Technology. Her research interests include the impact of gold nanoparticles on biological systems.

Matthew T. Gole received his B.S. degree in Chemistry at The College of New Jersey in Ewing, NJ, in 2016. He is currently a Ph.D. candidate in the Murphy group at UIUC. His research interests include the interactions of biomolecules with deformed 2D materials.

Daniel M. Hofmann received his B.S. degree in Chemistry from Millersville University in Pennsylvania in 2015. He is currently a Ph.D. candidate in the Murphy group at UIUC. His research interests include the synthesis and applications of bimetallic nanoparticles.

Khoi Nguyen L. Hoang is pursuing her Ph.D. in the Murphy group at UIUC. She graduated from Augsburg University in 2018 with a B.S. in Chemistry and Physics. Her research interests include interactions and transformations of nanoparticles in the environment.

Sophia M. McClain graduated with a B.S. degree in Chemistry from Indiana University-Bloomington in 2018. She is currently a Ph.D. student in the Murphy group at UIUC. Her research interests include biomolecular adsorption to gold nanoparticles and gold nanoparticle surface chemistry.

Sean M. Meyer is a second-year chemistry graduate student in the Murphy research group at UIUC. He received his B.Sc. in Chemistry from Texas Tech University in May 2017. His research focuses on using gold nanorods as SERS substrates and measuring their size-dependent optical properties.

Jacob G. Turner graduated with his B.S. degree in Chemistry from Saginaw Valley State University in 2016. He is currently a Ph.D. candidate in the Murphy group at UIUC. His research interests include the synthesis of gold nanorod composite nanomaterials.

Mahima Unnikrishnan completed her B.S.—M.S. dual degree in Chemistry from the Indian Institute of Science Education and Research, Thiruvananthapuram and joined the Ph.D. program in chemistry at UIUC in the fall of 2018. She works in the Murphy and Gruebele groups and studies the effect of nanoparticles on protein—protein interactions in cells.

Meng Wu is a Ph.D. candidate in chemistry at UIUC with Professor Murphy. He received his B.S degree in Chemistry from Fudan University in 2015. His research interests focus on surface chemistry on nanomaterials and protein coronas on nanoparticles.

Xi Zhang received her B.S. degree in Clinical Pharmacy at Fujian Medical University with an internship at the Second Hospital of Fuzhou in China in 2012. She received her Master of Medicine degree in Pharmaceutical Analysis at Fujian Medical University in 2015. She joined the Murphy research group in 2015 to pursue a Ph.D. degree in chemistry. Her research interests include the interaction and impact of gold nanoparticles on biological systems.

Yishu Zhang graduated with B.S. degrees in Chemistry and Biochemistry from the University of Minnesota-Duluth in 2017. She is a graduate student in the Murphy group at UIUC. Her research interests include measuring the impact of nanoparticles on cell behavior.

ACKNOWLEDGMENTS

This work was partially supported by the National Science Foundation under the Center for Sustainable Nanotechnology, CHE-1503408. The CSN is part of the Centers for Chemical Innovation Program. This research was partially supported by the NSF through the University of Illinois at Urbana-Champaign Materials Research Science and Engineering Center DMR- 1720633. We also thank NSF CHE-1608743 and the National Institutes of Health (R21 HL129115 and R01 GM125845) for support.

■ REFERENCES

- (1) Albanese, A.; Tang, P. S.; Chan, W. C. W. The Effect of Nanoparticle Size, Shape, and Surface Chemistry on Biological Systems. *Annu. Rev. Biomed. Eng.* **2012**, *14* (1), 1–16.
- (2) Zhang, S.; Gao, H.; Bao, G. Physical Principles of Nanoparticle Cellular Endocytosis. ACS Nano 2015, 9 (9), 8655–8671.

- (3) Longmire, M.; Choyke, P. L.; Kobayashi, H. Clearance Properties of Nano-Sized Particles and Molecules as Imaging Agents: Considerations and Caveats. *Nanomedicine* **2008**, 3 (5), 703–717.
- (4) Yu, M.; Zheng, J. Clearance Pathways and Tumor Targeting of Imaging Nanoparticles. ACS Nano 2015, 9 (7), 6655–6674.
- (5) Soo Choi, H.; Liu, W.; Misra, P.; Tanaka, E.; Zimmer, J. P.; Itty Ipe, B.; Bawendi, M. G.; Frangioni, J. V. Renal Clearance of Quantum Dots. *Nat. Biotechnol.* **2007**, 25 (10), 1165–1170.
- (6) Blanco, E.; Shen, H.; Ferrari, M. Principles of Nanoparticle Design for Overcoming Biological Barriers to Drug Delivery. *Nat. Biotechnol.* **2015**, 33 (9), 941–951.
- (7) Geng, Y.; Dalhaimer, P.; Cai, S.; Tsai, R.; Tewari, M.; Minko, T.; Discher, D. E. Shape Effects of Filaments Versus Spherical Particles in Flow and Drug Delivery. *Nat. Nanotechnol.* **2007**, 2 (4), 249–255.
- (8) Lauffer, M. A. The Size and Shape of Tobacco Mosaic Virus Particles 1. J. Am. Chem. Soc. 1944, 66 (7), 1188–1194.
- (9) Ashcroft, N. W.; Mermin, N. D. Solid State Physics; Saunders College/Holt, Rinehart and Winston: Philadelphia, PA, 1976.
- (10) Smith, A. M.; Nie, S. Semiconductor Nanocrystals: Structure, Properties, and Band Gap Engineering. *Acc. Chem. Res.* **2010**, 43 (2), 190–200.
- (11) Kelly, K. L.; Coronado, E.; Zhao, L. L.; Schatz, G. C. The Optical Properties of Metal Nanoparticles: The Influence of Size, Shape, and Dielectric Environment. *J. Phys. Chem. B* **2003**, *107* (3), 668–677.
- (12) Willets, K. A.; Van Duyne, R. P. Localized Surface Plasmon Resonance Spectroscopy and Sensing. *Annu. Rev. Phys. Chem.* **2007**, 58 (1), 267–297.
- (13) Jain, P. K.; Lee, K. S.; El-Sayed, I. H.; El-Sayed, M. A. Calculated Absorption and Scattering Properties of Gold Nanoparticles of Different Size, Shape, and Composition: Applications in Biological Imaging and Biomedicine. *J. Phys. Chem. B* **2006**, *110* (14), 7238–7248.
- (14) Burrows, N. D.; Lin, W.; Hinman, J. G.; Dennison, J. M.; Vartanian, A. M.; Abadeer, N. S.; Grzincic, E. M.; Jacob, L. M.; Li, J.; Murphy, C. J. Surface Chemistry of Gold Nanorods. *Langmuir* **2016**, 32 (39), 9905–9921.
- (15) Hinman, J. G.; Stork, A. J.; Varnell, J. A.; Gewirth, A. A.; Murphy, C. J. Seed Mediated Growth of Gold Nanorods: Towards Nanorod Matryoshkas. *Faraday Discuss.* **2016**, *191* (10), 9–33.
- (16) He, Y. Q.; Liu, S. P.; Kong, L.; Liu, Z. F. A Study on the Sizes and Concentrations of Gold Nanoparticles by Spectra of Absorption, Resonance Rayleigh Scattering and Resonance Non-Linear Scattering. *Spectrochim. Acta, Part A* **2005**, *61* (13–14), 2861–2866.
- (17) Yang, J. A.; Phan, H. T.; Vaidya, S.; Murphy, C. J. Nanovacuums: Nanoparticle Uptake and Differential Cellular Migration on a Carpet of Nanoparticles. *Nano Lett.* **2013**, *13* (5), 2295–2302.
- (18) Stiles, P. L.; Dieringer, J. A.; Shah, N. C.; Van Duyne, R. P. Surface-Enhanced Raman Spectroscopy. *Annu. Rev. Anal. Chem.* **2008**, *1* (1), 601–626.
- (19) Abadeer, N. S.; Murphy, C. J. Recent Progress in Cancer Thermal Therapy Using Gold Nanoparticles. *J. Phys. Chem. C* **2016**, 120 (9), 4691–4716.
- (20) Huang, X.; El-Sayed, I. H.; Qian, W.; El-Sayed, M. A. Cancer Cell Imaging and Photothermal Therapy in the Near-Infrared Region by Using Gold Nanorods. *J. Am. Chem. Soc.* **2006**, *128* (6), 2115–2120.
- (21) Sau, T. K.; Murphy, C. J. Seeded High Yield Synthesis of Short Au Nanorods in Aqueous Solution. *Langmuir* **2004**, *20* (15), 6414–6420.
- (22) Burrows, N. D.; Harvey, S.; Idesis, F. A.; Murphy, C. J. Understanding the Seed-Mediated Growth of Gold Nanorods Through a Fractional Factorial Design of Experiments. *Langmuir* **2017**, 33 (8), 1891–1907.
- (23) Chang, H.-H.; Murphy, C. J. Mini Gold Nanorods with Tunable Plasmonic Peaks Beyond 1000 nm. *Chem. Mater.* **2018**, *30* (4), 1427–1435.

(24) Vigderman, L.; Zubarev, E. R. High-Yield Synthesis of Gold Nanorods with Longitudinal SPR Peak Greater Than 1200 nm Using Hydroquinone as a Reducing Agent. Chem. Mater. 2013, 25 (8), 1450-1457.

- (25) Ye, X.; Zheng, C.; Chen, J.; Gao, Y.; Murray, C. B. Using Binary Surfactant Mixtures to Simultaneously Improve the Dimensional Tunability and Monodispersity in the Seeded Growth of Gold Nanorods. Nano Lett. 2013, 13 (2), 765-771.
- (26) Jia, H.; Fang, C.; Zhu, X.-M.; Ruan, Q.; Wang, Y.-X. J.; Wang, J. Synthesis of Absorption-Dominant Small Gold Nanorods and Their Plasmonic Properties. Langmuir 2015, 31 (26), 7418-7426.
- (27) Park, K.; Biswas, S.; Kanel, S.; Nepal, D.; Vaia, R. A. Engineering the Optical Properties of Gold Nanorods: Independent Tuning of Surface Plasmon Energy, Extinction Coefficient, and Scattering Cross Section. J. Phys. Chem. C 2014, 118 (11), 5918-5926.
- (28) Orendorff, C. J.; Murphy, C. J. Quantitation of Metal Content in the Silver-Assisted Growth of Gold Nanorods. J. Phys. Chem. B 2006, 110 (9), 3990-3994.
- (29) Hinman, J. G.; Turner, J. G.; Hofmann, D. M.; Murphy, C. J. Layer-by-Layer Synthesis of Conformal Metal-Organic Framework Shells on Gold Nanorods. Chem. Mater. 2018, 30 (20), 7255-7261.
- (30) Liu, B.-J.; Lin, K.-Q.; Hu, S.; Wang, X.; Lei, Z.-C.; Lin, H.-X.; Ren, B. Extraction of Absorption and Scattering Contribution of Metallic Nanoparticles Toward Rational Synthesis and Application. Anal. Chem. 2015, 87 (2), 1058-1065.
- (31) Nguyen, S. C.; Zhang, Q.; Manthiram, K.; Ye, X.; Lomont, J. P.; Harris, C. B.; Weller, H.; Alivisatos, A. P. Study of Heat Transfer Dynamics from Gold Nanorods to the Environment via Time-Resolved Infrared Spectroscopy. ACS Nano 2016, 10 (2), 2144-2151.
- (32) Abadeer, N. S.; Brennan, M. R.; Wilson, W. L.; Murphy, C. J. Distance and Plasmon Wavelength Dependent Fluorescence of Molecules Bound to Silica-Coated Gold Nanorods. ACS Nano 2014, 8 (8), 8392-8406.
- (33) Liu, J.; Detrembleur, C.; De Pauw-Gillet, M.-C.; Mornet, S.; Jérôme, C.; Duguet, E. Gold Nanorods Coated with Mesoporous Silica Shell as Drug Delivery System for Remote Near Infrared Light-Activated Release and Potential Phototherapy. Small 2015, 11 (19),
- (34) Gao, Z.; Burrows, N. D.; Valley, N. A.; Schatz, G. C.; Murphy, C. J.; Haynes, C. L. In Solution SERS Sensing Using Mesoporous Silica-Coated Gold Nanorods. Analyst 2016, 141 (17), 5088-5095.
- (35) Li, Y.; Jin, J.; Wang, D.; Lv, J.; Hou, K.; Liu, Y.; Chen, C.; Tang, Z. Coordination-Responsive Drug Release Inside Gold Nanorod@ Metal-Organic Framework Core-Shell Nanostructures for Near-Infrared-Induced Synergistic Chemo-Photothermal Therapy. Nano Res. 2018, 11 (6), 3294-3305.
- (36) Osterrieth, J. W. M.; Wright, D.; Noh, H.; Kung, C.-W.; Vulpe, D.; Li, A.; Park, J. E.; Van Duyne, R. P.; Moghadam, P. Z.; Baumberg, J. J.; Farha, O. K.; Fairen-Jimenez, D. Core-Shell Gold Nanorod@ Zirconium-Based Metal-Organic Framework Composites as in Situ Size-Selective Raman Probes. J. Am. Chem. Soc. 2019, 141 (9), 3893-
- (37) Xu, C.; Chen, F.; Valdovinos, H. F.; Jiang, D.; Goel, S.; Yu, B.; Sun, H.; Barnhart, T. E.; Moon, J. J.; Cai, W. Bacteria-Like Mesoporous Silica-Coated Gold Nanorods for Positron Emission Tomography and Photoacoustic Imaging-Guided Chemo-Photothermal Combined Therapy. Biomaterials 2018, 165, 56-65.
- (38) Furukawa, H.; Cordova, K. E.; O'Keeffe, M.; Yaghi, O. M. The Chemistry and Applications of Metal-Organic Frameworks. Science 2013, 341 (6149), 1230444.
- (39) Zeng, J.-Y.; Zhang, M.-K.; Peng, M.-Y.; Gong, D.; Zhang, X.-Z. Porphyrinic Metal-Organic Frameworks Coated Gold Nanorods as a Versatile Nanoplatform for Combined Photodynamic/Photothermal/ Chemotherapy of Tumor. Adv. Funct. Mater. 2018, 28 (8), 1705451.
- (40) Decher, G.; Hong, J. D.; Schmitt, J. Buildup of Ultrathin Multilayer Films by a Self-Assembly Process: III. Consecutively

Alternating Adsorption of Anionic and Cationic Polyelectrolytes on Charged Surfaces. Thin Solid Films 1992, 210-211, 831-835.

- (41) Gole, A.; Murphy, C. J. Polyelectrolyte-Coated Gold Nanorods: Synthesis, Characterization and Immobilization. Chem. Mater. 2005, 17 (6), 1325-1330.
- (42) Huang, J.; Park, J.; Wang, W.; Murphy, C. J.; Cahill, D. G. Ultrafast Thermal Analysis of Surface Functionalized Gold Nanorods in Aqueous Solution. ACS Nano 2013, 7 (1), 589-597.
- (43) Sivapalan, S. T.; Vella, J. H.; Yang, T. K.; Dalton, M. J.; Swiger, R. N.; Haley, J. E.; Cooper, T. M.; Urbas, A. M.; Tan, L.-S.; Murphy, C. J. Plasmonic Enhancement of the Two Photon Absorption Cross Section of an Organic Chromophore Using Polyelectrolyte-Coated Gold Nanorods. Langmuir 2012, 28 (24), 9147-9154.
- (44) Yang, J. A.; Murphy, C. J. Evidence for Patchy Lipid Layers on Gold Nanoparticle Surfaces. Langmuir 2012, 28 (12), 5404-5416.
- (45) Love, J. C.; Estroff, L. A.; Kriebel, J. K.; Nuzzo, R. G.; Whitesides, G. M. Self-Assembled Monolayers of Thiolates on Metals as a Form of Nanotechnology. Chem. Rev. 2005, 105 (4), 1103-1170.
- (46) Wu, M.; Vartanian, A. M.; Chong, G.; Pandiakumar, A. K.; Hamers, R. J.; Hernandez, R.; Murphy, C. J. Solution NMR Analysis of Ligand Environment in Quaternary Ammonium-Terminated Self-Assembled Monolayers on Gold Nanoparticles: The Effect of Surface Curvature and Ligand Structure. J. Am. Chem. Soc. 2019, 141 (10), 4316-4327.
- (47) Nuzzo, R. G.; Zegarski, B. R.; Dubois, L. H. Fundamental Studies of the Chemisorption of Organosulfur Compounds on Gold(111). Implications for Molecular Self-Assembly on Gold Surfaces. J. Am. Chem. Soc. 1987, 109 (3), 733-740.
- (48) Hinterwirth, H.; Kappel, S.; Waitz, T.; Prohaska, T.; Lindner, W.; Lämmerhofer, M. Quantifying Thiol Ligand Density of Self-Assembled Monolayers on Gold Nanoparticles by Inductively Coupled Plasma-Mass Spectrometry. ACS Nano 2013, 7 (2), 1129-1136.
- (49) Ivanov, M. R.; Haes, A. J. Anionic Functionalized Gold Nanoparticle Continuous Full Filling Separations: Importance of Sample Concentration. Anal. Chem. 2012, 84 (3), 1320-1326.
- (50) Smith, A. M.; Marbella, L. E.; Johnston, K. A.; Hartmann, M. J.; Crawford, S. E.; Kozycz, L. M.; Seferos, D. S.; Millstone, J. E. Quantitative Analysis of Thiolated Ligand Exchange on Gold Nanoparticles Monitored by ¹H NMR Spectroscopy. Anal. Chem. **2015**, 87 (5), 2771–2778.
- (51) Terrill, R. H.; Postlethwaite, T. A.; Chen, C.-H.; Poon, C.-D.; Terzis, A.; Chen, A.; Hutchison, J. E.; Clark, M. R.; Wignall, G.; Londono, J. D.; Superfine, R.; Falvo, M.; Johnson, C. S., Jr.; Samulski, E. T.; Murray, R. W. Monolayers in Three Dimensions: NMR, SAXS, Thermal, and Electron Hopping Studies of Alkanethiol Stabilized Gold Clusters. J. Am. Chem. Soc. 1995, 117 (50), 12537-12548.
- (52) Xia, X.; Yang, M.; Wang, Y.; Zheng, Y.; Li, Q.; Chen, J.; Xia, Y. Quantifying the Coverage Density of Poly(Ethylene Glycol) Chains on the Surface of Gold Nanostructures. ACS Nano 2012, 6 (1), 512-
- (53) Zhang, D.; Ansar, S. M. Ratiometric Surface Enhanced Raman Quantification of Ligand Adsorption onto a Gold Nanoparticle. Anal. Chem. 2010, 82 (13), 5910-5914.
- (54) Hill, H. D.; Millstone, J. E.; Banholzer, M. J.; Mirkin, C. A. The Role Radius of Curvature Plays in Thiolated Oligonucleotide Loading on Gold Nanoparticles. ACS Nano 2009, 3 (2), 418-424.
- (55) Docter, D.; Westmeier, D.; Markiewicz, M.; Stolte, S.; Knauer, S. K.; Stauber, R. H. The Nanoparticle Biomolecule Corona: Lessons Learned-Challenge Accepted? Chem. Soc. Rev. 2015, 44 (17), 6094-
- (56) Dennison, J. M.; Zupancic, J. M.; Lin, W.; Dwyer, J. H.; Murphy, C. J. Protein Adsorption to Charged Gold Nanospheres as a Function of Protein Deformability. Langmuir 2017, 33 (31), 7751-
- (57) Zhang, X.; Pandiakumar, A. K.; Hamers, R. J.; Murphy, C. J. Quantification of Lipid Corona Formation on Colloidal Nanoparticles from Lipid Vesicles. Anal. Chem. 2018, 90 (24), 14387-14394.

(58) Mahmoudi, M.; Lohse, S. E.; Murphy, C. J.; Fathizadeh, A.; Montazeri, A.; Suslick, K. S. Variation of Protein Corona Composition of Gold Nanoparticles Following Plasmonic Heating. *Nano Lett.* **2014**, 14 (1), 6–12.

- (59) Yeo, E. L. L.; Thong, P. S. P.; Soo, K. C.; Kah, J. C. Y. Protein Corona in Drug Delivery for Multimodal Cancer Therapy in Vivo. *Nanoscale* **2018**, *10* (5), 2461–2472.
- (60) Ghosh, P.; Han, G.; De, M.; Kim, C. K.; Rotello, V. M. Gold Nanoparticles in Delivery Applications. *Adv. Drug Delivery Rev.* **2008**, 60 (11), 1307–1315.
- (61) Lin, W.; Murphy, C. J. A Demonstration of Le Chatelier's Principle on the Nanoscale. *ACS Cent. Sci.* **2017**, 3 (10), 1096–1102. (62) Norman, R. S.; Stone, J. W.; Gole, A.; Murphy, C. J.; Sabo-Attwood, T. L. Targeted Photothermal Lysis of the Pathogenic Bacteria, *Pseudomonas aeruginosa*, with Gold Nanorods. *Nano Lett.* **2008**, 8 (1), 302–306.
- (63) Yang, T.; Wang, D.; Liu, X. Assembled Gold Nanorods for the Photothermal Killing of Bacteria. *Colloids Surf.*, B **2019**, 173, 833–841
- (64) Hu, D.; Li, H.; Wang, B.; Ye, Z.; Lei, W.; Jia, F.; Jin, Q.; Ren, K.-F.; Ji, J. Surface-Adaptive Gold Nanoparticles with Effective Adherence and Enhanced Photothermal Ablation of Methicillin-Resistant Staphylococcus aureusBiofilm. *ACS Nano* **2017**, *11* (9), 9330–9339.
- (65) Grzincic, E. M.; Murphy, C. J. Gold Nanorods Indirectly Promote Migration of Metastatic Human Breast Cancer Cells in Three-Dimensional Cultures. *ACS Nano* **2015**, 9 (7), 6801–6816.
- (66) Grzincic, E. M.; Yang, J. A.; Drnevich, J.; Falagan-Lotsch, P.; Murphy, C. J. Global Transcriptomic Analysis of Model Human Cell Lines Exposed to Surface-Modified Gold Nanoparticles: The Effect of Surface Chemistry. *Nanoscale* **2015**, *7* (4), 1349–1362.
- (67) Falagan-Lotsch, P.; Grzincic, E. M.; Murphy, C. J. One Low-Dose Exposure of Gold Nanoparticles Induces Long-Term Changes in Human Cells. *Proc. Natl. Acad. Sci. U. S. A.* **2016**, *113* (47), 13318–13323.
- (68) Ali, M. R. K.; Rahman, M. A.; Wu, Y.; Han, T.; Peng, X.; Mackey, M. A.; Wang, D.; Shin, H. J.; Chen, Z. G.; Xiao, H.; Wu, R.; Tang, Y.; Shin, D. M.; El-Sayed, M. A. Efficacy, Long-Term Toxicity, and Mechanistic Studies of Gold Nanorods Photothermal Therapy of Cancer in Xenograft Mice. *Proc. Natl. Acad. Sci. U. S. A.* 2017, 114 (15), E3110–E3118.
- (69) Lohse, S. E.; Abadeer, N. S.; Zoloty, M.; White, J. C.; Newman, L. A.; Murphy, C. J. Nanomaterial Probes in the Environment: Gold Nanoparticle Soil Retention and Environmental Stability as a Function of Surface Chemistry. ACS Sustainable Chem. Eng. 2017, 5 (12), 11451–11458.
- (70) Buchman, J. T.; Rahnamoun, A.; Landy, K. M.; Zhang, X.; Vartanian, A. M.; Jacob, L. M.; Murphy, C. J.; Hernandez, R.; Haynes, C. L. Using an Environmentally-Relevant Panel of Gram-Negative Bacteria to Assess the Toxicity of Polyallylamine Hydrochloride-Wrapped Gold Nanoparticles. *Environ. Sci.: Nano* **2018**, *5*, 279–288.
- (71) Metch, J. W.; Burrows, N. D.; Murphy, C. J.; Pruden, A.; Vikesland, P. J. Metagenomic Analysis of Microbial Communities Yields Insight into Impacts of Nanoparticle Design. *Nat. Nanotechnol.* **2018**, *13*, 253–259.
- (72) Qi, L.; Ge, Y.; Xia, T.; He, J.-Z.; Shen, C.; Wang, J.; Liu, Y.-J. Rare Earth Oxide Nanoparticles Promote Soil Microbial Antibiotic Resistance by Selectively Enriching Antibiotic Resistance Genes. *Environ. Sci.: Nano* **2019**, *6* (2), 456–466.
- (73) Burns, J. M.; Pennington, P. L.; Sisco, P. N.; Frey, R.; Kashiwada, S.; Fulton, M. H.; Scott, G. I.; Decho, A. W.; Murphy, C. J.; Shaw, T. J.; Ferry, J. L. Surface Charge Controls the Fate of Au Nanorods in Saline Estuaries. *Environ. Sci. Technol.* **2013**, 47 (22), 12844–12851.
- (74) Ferry, J. L.; Craig, P.; Hexel, C.; Sisco, P.; Frey, R.; Pennington, P. L.; Fulton, M. H.; Scott, I. G.; Decho, A. W.; Kashiwada, S.; Murphy, C. J.; Shaw, T. J. Transfer of Gold Nanoparticles from the Water Column to the Estuarine Food Web. *Nat. Nanotechnol.* **2009**, *4* (7), 441–444.

- (75) Avellan, A.; Simonin, M.; McGivney, E.; Bossa, N.; Spielman-Sun, E.; Rocca, J. D.; Bernhardt, E. S.; Geitner, N. K.; Unrine, J. M.; Wiesner, M. R.; Lowry, G. V. Gold Nanoparticle Biodissolution by a Freshwater Macrophyte and Its Associated Microbiome. *Nat. Nanotechnol.* **2018**, *13*, 1072–1077.
- (76) Zimmermann, M.; Zimmermann-Kogadeeva, M.; Wegmann, R.; Goodman, A. L. Mapping Human Microbiome Drug Metabolism by Gut Bacteria and Their Genes. *Nature* **2019**, *570*, 462–467.